MacDonald, Iain T.; Vincent, Christopher E.; Thorne, Peter D.; Moate, Benjamin D.. 2013 Acoustic scattering from a suspension of flocculated sediments. *Journal of Geophysical Research: Oceans*, 118 (5). 2581-2594. 10.1002/jgrc.20197

MacDonald, Iain T.; Vincent, Christopher E.; Thorne, Peter D.; Moate, Benjamin D.. 2013 Acoustic scattering from a suspension of flocculated sediments. *Journal of Geophysical Research: Oceans*, 118 (5). 2581-2594. 10.1002/jgrc.20197

JOURNAL OF GEOPHYSICAL RESEARCH: OCEANS, VOL. 118, 2581–2594, doi:10.1002/jgrc.20197, 2013

Acoustic scattering from a suspension of flocculated sediments

Iain T. MacDonald,[1,2] Christopher E. Vincent,[1] Peter D. Thorne,[3] and Benjamin D. Moate[3]

Received 7 March 2013; revised 7 March 2013; accepted 9 April 2013; published 22 May 2013

[1] A series of controlled laboratory experiments have been conducted to investigate the backscatter of high frequency sound (3–5 MHz) from suspensions of fine sediment in its unflocculated (primary) state and at various levels of flocculation. The size and fall-velocity distributions of the flocs were determined using an optical system and a settling tube, thus allowing floc density to be determined. The measurements have conclusively demonstrated that the acoustic properties of the flocculated particles are not solely controlled by the primary particles; some aspect of the floc structure is influencing the scattering characteristics. The overall trend is for the form function (K_s) to increase as the degree of flocculation increases. This trend was also observed in the total scattering cross section ($\overline{\sigma_t}$) but this result is dependent on the assumption that viscous absorption for flocculated particles is negligible. The measured scattering properties are compared to the predicted values from two theoretical models, the elastic (ES) and fluid sphere (FS) models. While the results show that, in their current form, neither model is capable of adequately representing the scattering characteristics of a suspension of flocculated particles, the two models did provide upper (ES) and lower (FS) bounds to the measurements. In terms of the operational use of acoustics to measure the concentration of flocculated sediments, empirical relationships could be fitted to the observations but, until a better theoretical understanding of how sound interacts with flocculated particles is achieved, the fitting of such empirical relations may be somewhat premature.

Citation: MacDonald, I. T., C. E. Vincent, P. D. Thorne, and B. D. Moate (2013), Acoustic scattering from a suspension of flocculated sediments, *J. Geophys. Res. Oceans*, *118*, 2581–2594, doi:10.1002/jgrc.20197.

1. Introduction

[2] Flocculated particles in the marine environment are one of today's great challenges for sediment transport studies. In marine waters, suspended particles rarely exist in their primary state; instead they are typically aggregated, heterogeneous assemblages of mineral grains, biogenic debris, bacteria, and organic material. The pronounced influence suspended fine particles exert on water quality in estuaries and coastal seas is well known [*Eisma et al.*, 1991; *Winterwerp*, 2002]. A floc or aggregate may constitute of the order 10^6 individual particles and floc size can range over 4 orders of magnitude within any one floc population, from clay particles of 1 μm diameter to macrofloc of several millimeters. As flocs grow more ambient fluid is trapped in the interstitial spaces between the particles. Therefore, floc density is inversely proportional to floc size, with large flocs having a density only slightly greater than that of the ambient fluid [*Dyer and Manning*, 1999; *Khelifa and Hill*, 2006; *Manning and Bass*, 2006].

[3] Acoustic instruments are routinely used in coastal and estuarine studies for measuring currents and current profiles. Increasingly, such acoustic instruments are also being used to simultaneously estimate suspended-sediment concentration and concentration profiles using the strength of the backscattered acoustic signal, from which sediment transport is calculated [*Deines*, 1999; *Fugate and Friedrichs*, 2002]. This method typically relies on taking a large number of water samples and building an empirical relationship between mass concentration of suspended sediment and acoustic backscatter intensity. The approach, however, provides little or no information about the degree of sediment flocculation. An alternative method, which can yield particle size information, is based on the inversion of the backscatter equation for suspended noncohesive sand. Such inversions rely on the specification of two key parameters that describe the scattering characteristics of the suspended particles: the ensemble backscatter form function (K_s) and the ensemble total scattering cross section ($\overline{\sigma_t}$). As K_s increases, the voltage recorded by the receiver increases because more energy is scattered back to the sensor; whereas as $\overline{\sigma_t}$ increases, the voltage decreases as more energy is scattered away from the sensor. For noncohesive

Additional supporting information may be found in the online version of this article.

[1]School of Environment Sciences, University of East Anglia, Norwich, UK.
[2]Now at National Institute of Water and Atmospheric Research, Hamilton, Waikato, New Zealand.
[3]National Oceanography Centre, Liverpool, UK.

Corresponding author: I. T. MacDonald, National Institute of Water and Atmospheric Research, Hamilton, Waikato 3216, New Zealand. (i.macdonald@niwa.co.nz)

2169-9275/13/10.1002/jgrc.20197

sand particles, these terms are well defined [*Moate and Thorne*, 2009; *Thorne and Hanes*, 2002]; however, the suitability of such relationships for cohesive fine sediments is yet to be determined.

[4] Here we present results from a series of controlled laboratory experiments to examine how the particle scattering characteristics change as a result of flocculation. Measured values for K_s and $\overline{\sigma_t}$ are compared to predicted values from two theoretical models, the elastic sphere (ES) and fluid sphere (FS) models.

2. Theory

[5] When multiple scattering can be ignored the incoherent ensemble mean-square voltage (V_{rms}) due to backscattering from particles at range r by an acoustic backscatter sensor (ABS) can be written as [*Sheng and Hay*, 1988; *Thorne and Hanes*, 2002]

$$V_{\mathrm{rms}}(r) = \frac{K_t K_s N^{1/2}}{r\psi} e^{-2r\left(\alpha_w+\alpha_v+\frac{N}{2}\overline{\sigma_t}\right)}, \tag{1}$$

where

$$K_s = \left(\int_0^\infty a^2 f^2(x) n(a)\mathrm{d}a\right)^{1/2}, \tag{2}$$

$$\overline{\sigma_t} = \int_0^\infty \sigma_t(a) n(a)\mathrm{d}a, \tag{3}$$

$$K_t = \mathrm{RT}_v p_0 r_0 \left(\frac{\pi\tau c}{4}\right)^{1/2} \left(\int_0^{\pi/2} D^4(\theta)\sin\theta\mathrm{d}\theta\right)^{1/2}, \tag{4}$$

where N is the number of particles per unit volume, ψ is the near-field correction, which accounts for the nonspherical spreading that occurs near the transducers [*Downing et al.*, 1995], α_w is the attenuation due to water absorption, α_v is the attenuation due to viscous absorption, a is the particle radius, $f(x)$ is the form function that corresponds to the dimensionless particle parameter x where $x = ka$ and k is acoustic wavenumber, $n(a)$ is the particle size probability density function, and $\sigma_t(a)$ is the total scattering cross section of a single particle of radius a. For the simple case of a homogeneous suspension with a single particle size and density, equations (2) and (3) reduce to $K_s = af(x)$ and $\overline{\sigma_t} = \sigma_t(a)$, respectively. The K_t term contains system parameters: R is the receive sensitivity, T_v is the electronic gain of the system, p_0 is the reference pressure at distance r_0 from the transducer face, $D(\theta)$ is transducer directivity, θ is the angle that subtends the acoustic axis, c is the speed of sound in water, and τ is the pulse duration.

[6] Taking the natural logarithm of equation (1) yields [*Moate and Thorne*, 2009; *Thorne and Buckingham*, 2004]

$$\ln(V_{\mathrm{rms}} r\psi) = \ln\left(K_t K_s N^{1/2}\right) - 2r\left(\alpha_w + \alpha_v + \frac{N}{2}\overline{\sigma_t}\right). \tag{5}$$

[7] Equation (5) is now a linear function of $\ln(V_{\mathrm{rms}} r\psi)$ versus r, from which the following expressions for $\overline{\sigma_t}$ and K_s can be derived

$$\overline{\sigma_t} = \frac{-2(\alpha_w+\alpha_v)-\kappa}{N}, \tag{6}$$

$$K_s = \frac{e^{\eta}}{K_t N^{1/2}}, \tag{7}$$

where κ and η are the slope and intercept, respectively derived from the fit of equation (5) to ABS observations.

[8] For comparative purposes the measured values for $\overline{\sigma_t}$ and K_s are compared to the predicted values from two theoretical models: the ES and FS models. These two models were selected as they potentially span the transition from solid (primary) particles to large fluid-like flocs. The models provide expressions for $f(x)$ and $\sigma_t(x)$ which, after substitution into equations (2) and (3) yield $\overline{\sigma_t}$ and K_s. Expressions for $f(x)$ and $\sigma_t(x)$ for the ES and FS models are shown in equations (8)–(11).

$$f^{\mathrm{ES}}(x) = \frac{2}{ix}\sum_{q=0}^{\infty}(-1)^q(2q+1)b_q, \tag{8}$$

$$\sigma_t^{\mathrm{ES}}(x) = \frac{4\pi a^2}{x^2}\sum_{q=0}^{\infty}(2q+1)|b_q|^2, \tag{9}$$

$$f^{\mathrm{FS}}(x) = \left|\frac{2}{x}\sum_{q=0}^{\infty}(-1)^q(2q+1)/\left(1+ic_q\right)\right|, \tag{10}$$

$$\sigma_t^{\mathrm{FS}}(x) = \frac{4\pi a^2}{x^2}\sum_{q=0}^{\infty}(2q+1)/\left(1+c_q^2\right), \tag{11}$$

where k is the wave number of sound in water, $i = \sqrt{-1}$, b_q [*Gaunaurd and Überall*, 1983] and c_q [*Anderson*, 1950] are complex functions involving Bessel and Hankel functions and their derivatives, for completeness, expression for b_q and c_q are provided in Appendix A.

3. Methods

3.1. Experimental Arrangement

[9] A series of laboratory experiments was conducted to measure the acoustic backscatter from suspensions of kaolin (Specwhite™ SiO_2(47%), Al_2O_3 (38%), density 2650 kg/m^3) in a well-mixed 120 l recirculation tank (Figure 1). Flocculation was controlled through the incremental addition of a commercial flocculant (MAGNAFLOC®). Five mass concentrations were used, nominally 0.2, 0.4, 0.8, 1.6, and 3.2 g/l. The actual concentration was measured gravimetrically at four locations down the tank at five times throughout each experimental run. The measurements showed that the kaolin was uniformly distributed to ±5% throughout the tank.

[10] Acoustic backscatter was measured using an Aquatec Aquascat-1000™ at acoustic frequencies of 3, 4 and 5 MHz. The acoustic "ping" rate was set to 16 Hz, with

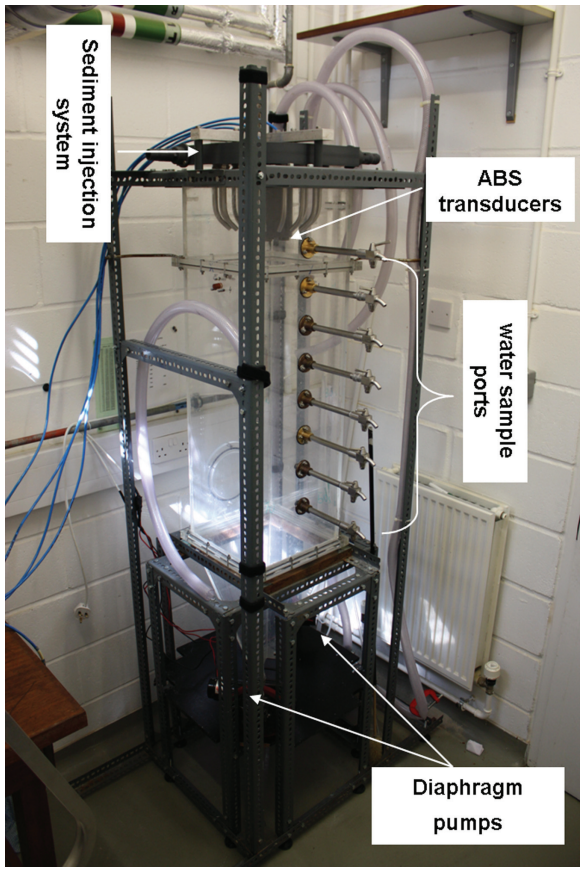

Figure 1. ABS recirculation tank.

backscatter profiles at 0.01 m intervals over a range of 0.70 m.

[11] The size distribution of the "primary particles" of kaolin was determined using a Malvern MasterSizer 2000^{TM}. The floc size and fall-speed distributions for the flocculated suspension were determined using the optical FLOCView system, which is described later.

[12] Each run took place over a period of three days. First, the tank was filled with deionized-microfiltered water. Once filled, the water was recirculated in the tank for 24 h, which allowed the water to degas and reach room temperature. After 24 h, 10 min of ABS measurements were made to determine the background signal level. Next, the ultrasonically dispersed, unflocculated ("primary") kaolin particles were added to the tank. To ensure that the particles were thoroughly mixed and a homogenous suspension was achieved, the tank was mixed for a further 21 h. After this mixing period, 20 min of ABS measurements were made to determine the scattering signal of the primary kaolin particles. Immediately after the 20 min measurement period, four water samples at 1, 10, 30 cm and 70 cm below the level of the acoustic transducers were collected from the centre of the tank. The suspended sediment concentration was later determined by gravimetric analysis of the water samples.

[13] After collecting the water samples, the MAGNAFLOC flocculant was added. To allow sufficient time for flocculation to occur, the tank was mixed for 110 min. After this mixing period, 10 min of ABS measurements were made to determine the scattering signal at floc level 1 (FL1), corresponding to the first addition of MAGNAFLOC.

[14] The floc size distribution and settling speed distribution at FL1 were estimated at the end of the ABS measurement period using FLOCView. This consisted of a 0.6 m high settling column, near the bottom of which was a 4 megapixel camera and macrolens which recorded images at up to a rate of 30 Hz. The instrument is shown in Figure 2a. A sample was carefully extracted from the tank and transferred to the settling column using a wide-mouthed (8 mm internal diameter) pipette. Samples were taken from the centre of the tank at a depth of approximately 35 cm below the level of the transducer; samples were drawn into the pipette slowly to minimize damage to the flocs. The pipette was then carefully lifted from the tank and placed so that the tip of the pipette was located just below the water surface in the settling column. Under gravity, the flocs then settled vertically out of the pipette and into the settling column. The sample transfer was made as quickly as possible to minimize the potential for additional flocculation that might occur once the kaolin suspension was no longer subject to the turbulent shear present in the mixing tank. The elapsed time between the start of drawing fluid into the pipette to collecting FLOCView images (containing flocs) was typically about 1–2 min. Figure 2b shows a typical

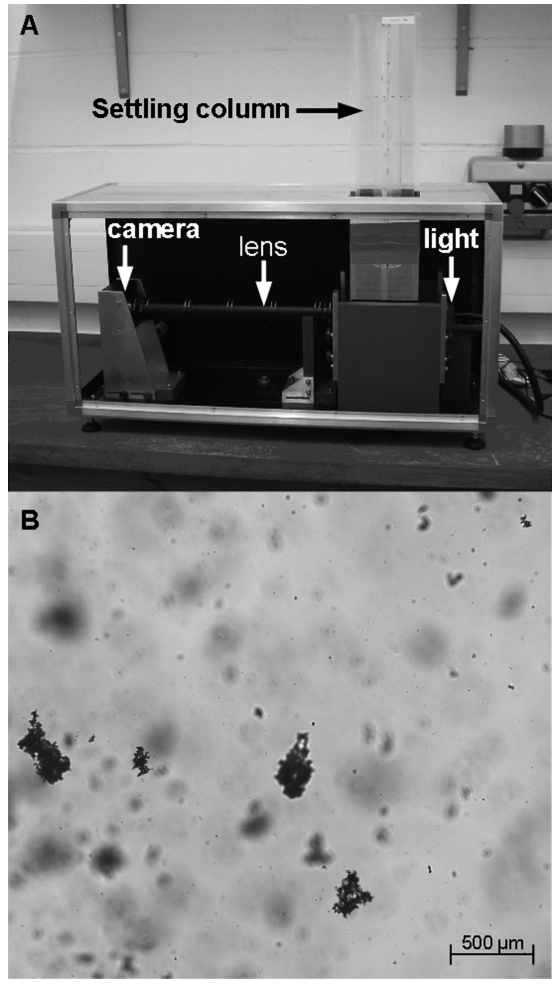

Figure 2. (a) FLOCView setup. (b) FLOCView image.

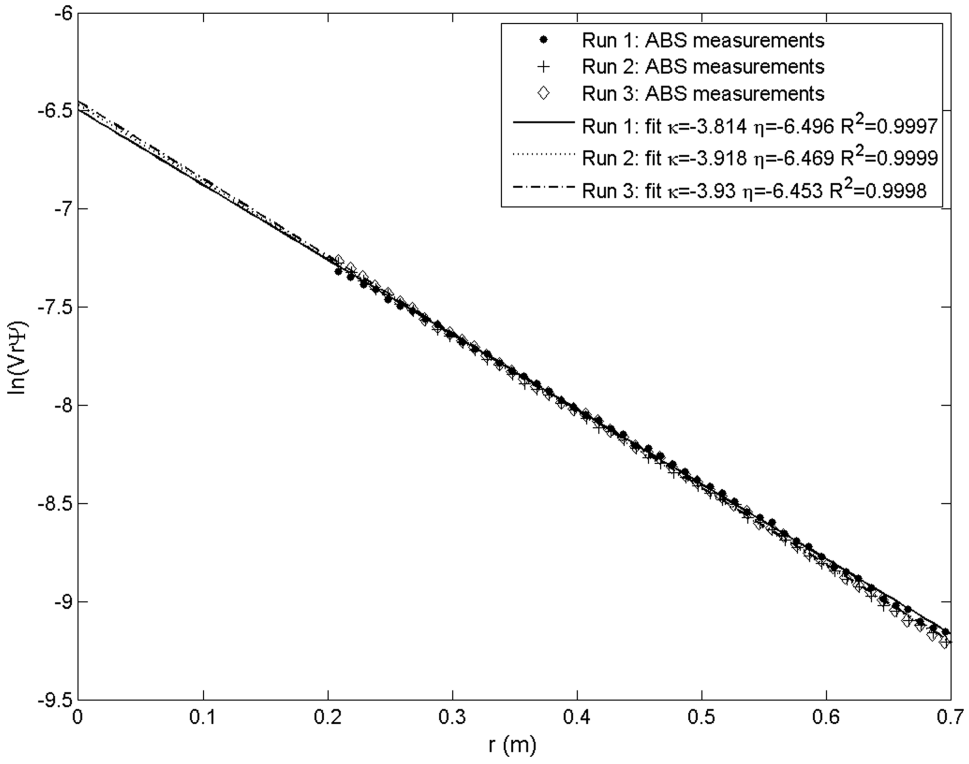

Figure 3. ABS measurements of $\ln(V_{\mathrm{rms}} r\psi)$ versus r for the three runs at 3.2 g/l for FL2 for the 5 MHz transducer.

FLOCView image. An automatic particle recognition system was developed to identify particles and to track the particles through a sequence of images, from which floc settling speed is estimated.

[15] The sequence of water samples, adding flocculant, mixing period, ABS measurements, and floc size and settling speed measurements was repeated a further three times to obtain floc levels 2, 3, and 4 (FL2, FL3, and FL4), corresponding to each extra addition of MAGNAFLOC. Runs were repeated three times for each concentration.

3.2. Data Processing

3.2.1. Obtaining Estimates for K_s and $\overline{\sigma_t}$ From ABS Measurements

[16] In order to evaluate equations (6) and (7), values for κ, η, α_w, α_v, K_t and N are required. Aside from α_w which can be obtained directly from literature [*Richards et al*., 1996], the other terms were evaluated as follows.

3.2.1.1. κ and η

[17] Figure 3 shows an example of the fit of equation (5) to ABS observations from which κ and η were estimated as described previously. The data shown are for the three runs at 3.2 g/l for FL2 for the 5 MHz transducer. Following *Thorne and Buckingham* [2004] the first 0.2 m of ABS data were excluded from the analysis in order to avoid potential problems with crosstalk and inaccuracies in the near field correction. Furthermore, values for κ and η were rejected when the coefficient of determination (R^2) was less than 0.95.

3.2.1.2. K_t

[18] The system constant K_t was evaluated using the calibration method of *Betteridge et al*. [2008]. Over the course of the experiments the calibration process was performed on three separate occasions. On each of these three occasions, the calibration was performed at two different sediment mass concentrations (0.5 and 1.0 g/l). The results of the calibration are shown in Figure 4, which shows profiles of K_t with range. The figure shows that aside from the region close to the transducer which is affected by crosstalk and inaccuracies in the near field correction that K_t is constant with range. The dotted lines in the figures are the K_t value obtained from averaging the calibration data for each frequency over the range 0.3–0.8 m. It is these values that are used for K_t.

3.2.1.3. N

[19] The suspended sediment mass concentration (M) is related to the number of particles per unit volume (N) as

$$M = N \int_0^\infty v(a)\rho(a)n(a)\mathrm{d}a, \tag{12}$$

where $v(a)$ and $\rho(a)$ are the volume and density, respectively of a particle of radius a.

[20] Under the assumption that the particles are spherical, N is given by

$$N = 3M \Big/ \left[4\pi \int_0^\infty a^3 \rho(a) n(a) \mathrm{d}a \right]. \tag{13}$$

[21] For noncohesive sediments, e.g., marine quartz sands, equation (13) is relatively easy to evaluate, since particle density is constant and calculating $n(a)$ is

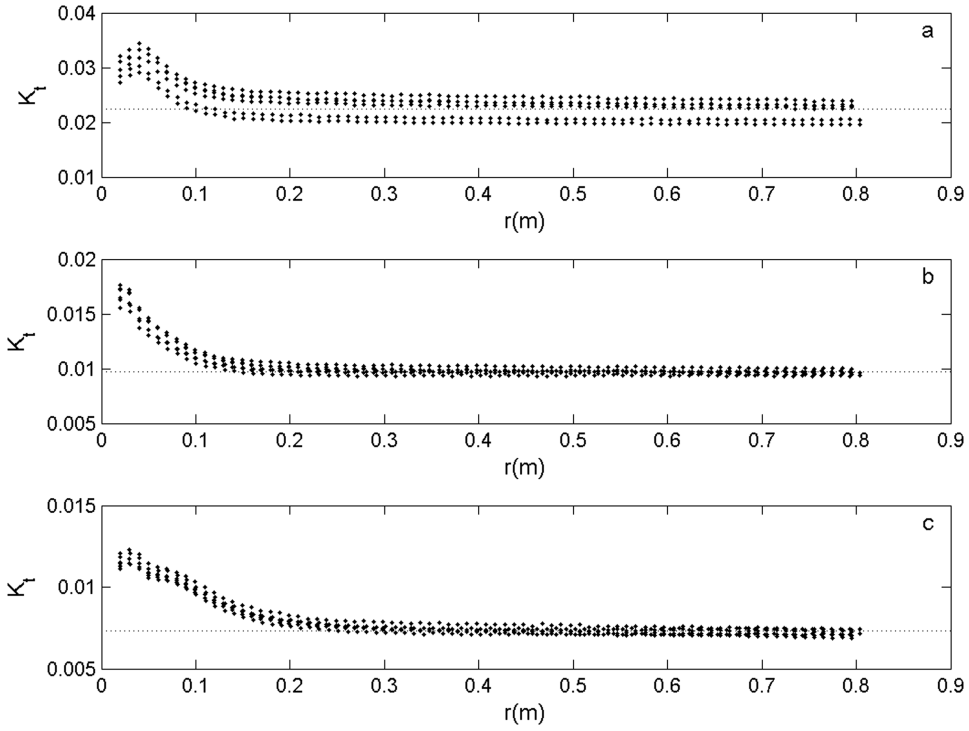

Figure 4. Measurements of K_t with range at (a) 3 MHz, (b) 4 MHz, and (c) 5 MHz. The dotted lines in the figures are the K_t values obtained from averaging the calibration data for each frequency over the range 0.3–0.8 m.

reasonably straightforward, e.g., through traditional techniques such as sieving. For the asymptotic case of uniform spherical grains of a single size, equation (13) reduces simply to $N = 3M/(4\pi a^3\rho)$. In contrast, for flocculated sediments density decreases with floc size. Furthermore, flocs are fragile and susceptible to breakage, and therefore $n(a)$ cannot be obtained through sieving.

[22] In order to obtain $\rho(a)$ and $n(a)$ so that N could be determined, the FLOCView system was employed. Optical systems [*Dyer and Manning*, 1999; *Fennessy et al*., 1994; *Manning and Dyer*, 1999, 2002; *Mikkelsen et al*., 2005; *Smith and Friedrichs*, 2011] such as FLOCView are extensively used in flocculation studies to measure various floc properties (e.g., size, shape, settling velocity, density). What follows is a description of the image processing procedure that ultimately yields $\rho(a)$ and $n(a)$ and therefore N.

[23] The automatic particle recognition system, which identifies and tracks particles, consists of two steps. The first involves segmentation of the FLOCView images to distinguish individual particles from the background. To do this the binary threshold method of *Otsu* [1979] was used. From the binary image, various particle parameters (size, shape, location) can be extracted; the two of most importance here are the two-dimensional projected area (A) and the particle location (centroid).

[24] The particle centroids were used to track the particles through consecutive images by minimizing the total squared displacement between all identified particles. This step was then repeated for all images within a settling experiment. Some simple additional intensity thresholding was necessary to ensure that only "in-focus" particles were included in the analyses.

[25] At the end of the particle recognition and tracking step, a list of frame number, centroid position and A for each tracked particle was generated. With the distance a particle moved between consecutive images and the time between images both known, the settling velocity (w_s) of the particle can be determined. As a single particle is tracked through multiple images, the final step was to produce average particle quantities. Therefore, all quantities derived from FLOCView presented here are averages from each particle realization.

[26] At this stage of the analyses quantities derived from FLOCView are expressed in terms of pixel dimensions. In order to convert from pixel units to IS units, FLOCView was calibrated by taking images of a glass calibration slide. The calibration slide consisted of a grid of circles each with an area of 3.06×10^{-9} m^2. From image analysis, the average number of pixels making up each circle was calculated to be 907; thus the area of each pixel was 3.38×10^{-12} m^2 (1.84 μm × 1.84 μm).

[27] Due to the irregular morphologies of flocs (see Figure 2b) the definition of floc size is somewhat problematic. Following the works of [*Graham and Nimmo Smith*, 2010; *Manning and Bass*, 2006] the definition of the equivalent spherical radius is adopted, where a is given by

$$a = \sqrt{\frac{A}{\pi}} \tag{14}$$

[28] Figure 5a shows an example of a size distribution obtained from the image analysis procedure. In order to calculate $n(a)$ a log-normal distribution was fitted to the data using the maximum likelihood estimate method. The

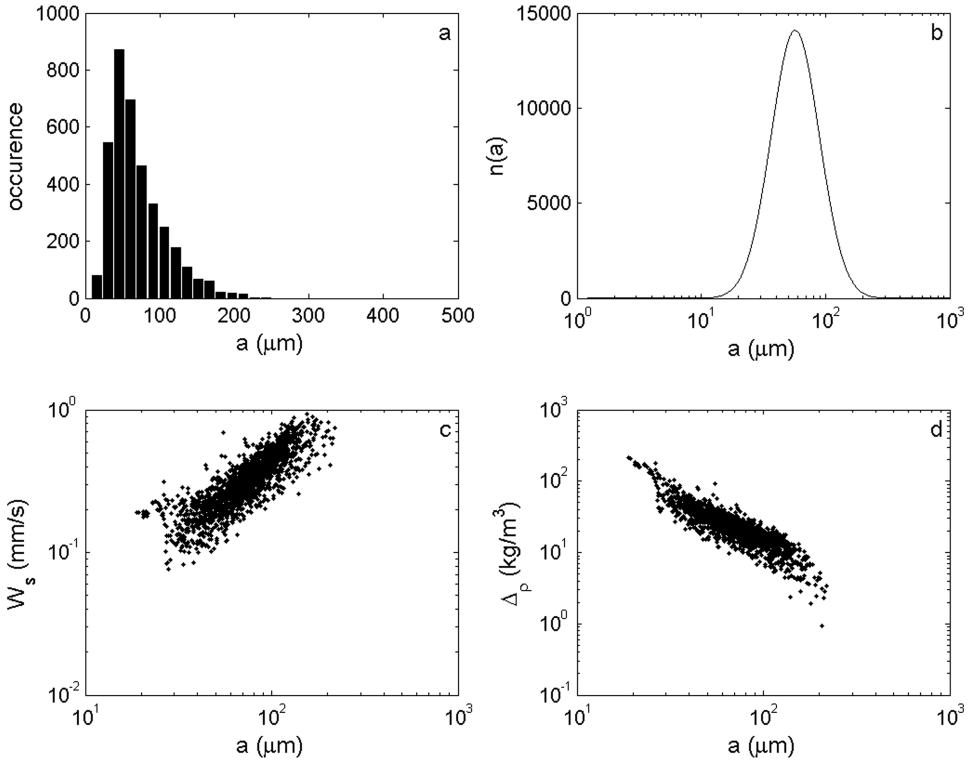

Figure 5. FLOCView results for run 1, 3.2 g/l, FL1. (a) Particle size distribution. (b) Particle size probability density function. (c) Settling speed distribution. (d) Effective density distribution.

result of a fit to the size distribution shown in Figure 5a is shown in Figure 5b.

[29] Figure 5c shows the settling speed data that correspond to the size distribution shown in Figure 5a. With a and w_s known, the effective density ($\Delta\rho$) of the flocs can be estimated from a rearranged version of Stokes law:

$$\Delta\rho = \rho_f - \rho_w = \frac{18 w_s \mu}{g d^2} \tag{15}$$

where ρ_f is the density of the floc, ρ_w is the water density (assumed to be 1000 kg/m^3), g is the acceleration due to gravity and μ is the dynamic viscosity.

[30] Figure 5d shows the density estimates using the settling velocity data shown in Figure 5c. Figure 5d shows a decrease in floc density with floc size, with the largest flocs having densities of around 1001 kg/m^3.

3.2.1.4. Viscous Absorption (α_v)

[31] Using *Urick*'s [1948] expression, acoustic attenuation due to viscous absorption for a suspension of spherical particles of radius a is given by

$$\alpha_v = \frac{\varepsilon k (\gamma - 1)^2}{2} \left(\frac{s}{s^2 + (\gamma + \delta)^2} \right), \tag{16}$$

where

$$s = \frac{9}{4\beta a}\left(1 + \frac{1}{\beta a}\right) \delta = \frac{1}{2}\left(1 + \frac{9}{2\beta a}\right),$$

with $\gamma = \rho(a)/\rho_w$ and $\beta = \sqrt{\omega/2\nu}$, where ω is the acoustic angular frequency, ν is the kinematic viscosity of the ambient fluid, and ε is the volume concentration of scatterers. Equation (16) predicts that the viscous absorption depends linearly on sediment concentration. Experimental observations [*Urick*, 1948] using kaolin have shown that this assumption is valid up to mass concentrations of *ca*. 200 g/l (the maximum concentration considered here is 3.2 g/l).

[32] Figure 6 investigates the relative importance of the two attenuation terms (α_v and α_w) that are required to determine $\overline{\sigma_t}$. Figure 6a shows the ratio of viscous absorption to water absorption (i.e., α_v/α_w) as a function of particle radius (a) for the three frequencies used in this study. In Figure 6a, α_v was calculated using a particle density of 2650 kg/m^3 (i.e., the density of kaolin) and a suspended sediment concentration of 3.2 g/l. α_w was calculated for freshwater at a temperature of 25°C. Figure 6a shows that α_v is significantly larger than α_w in the primary particle range, but for the range of flocculated particle sizes of interest here, α_w is larger than α_v. However, as an upper limit α_v is ca. 20% of the value of α_w, α_v is thus too large to be ignored. However, as shown in Figure 5d flocs have densities which are considerably less than 2650 kg/m^3. As floc density decreases with increase floc size (Figure 6b) α_w becomes by far the dominant attenuation mechanism. As will be shown shortly (see Figure 8), the majority of flocs in this study have densities lower than 1100 kg/m^3, in which case is α_v negligible. We therefore conclude that the attenuation due to viscous absorption must be taken into account for primary particles, but can be neglected (i.e., α_v=0) for flocs. The implications for this assumption are explored further in the discussion section.

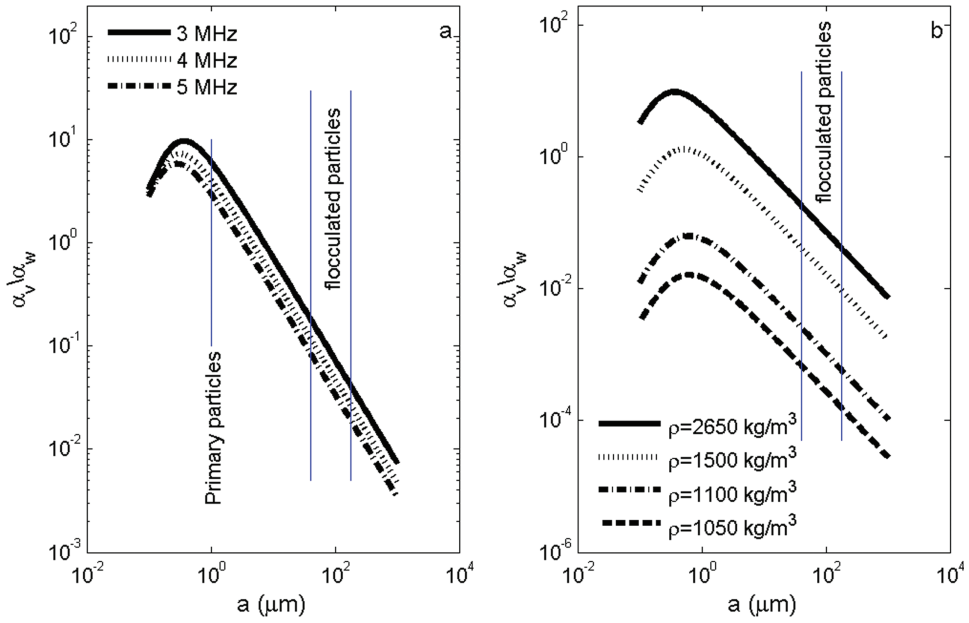

Figure 6. (a) Ratio of viscous absorption to water absorption (i.e., α_v/α_w) as a function of particle radius for the three transducer frequencies used in this study. (b) α_v/α_w for particles with densities of 2650, 1500, 1100, and 1050 kg/m^3 for the 3 MHz transducer and a mass concentration of 3.2 g/l.

4. Results

4.1. Size Distributions

4.1.1. Primary Particles

[33] The size distributions of the primary kaolin particles measurement by the Malvern MasterSizer are shown Figure 7. The distribution labelled "raw" in Figure 7 is of a sample taken from the kaolin used in the experiments. The "raw" kaolin sample was continuously dispersed (by ultrasound) while the particle size distribution was measured, and therefore represents the distribution of the unflocculated primary particles. The remaining two distributions were measured from water samples taken from the recirculating tank immediately after the 20 min period of ABS measurements of the primary particles. The sample was transferred to the MasterSizer and measured as quickly as possible to minimize any potential changes to the particle size distribution. Figure 7 shows the distributions measured for the samples taken immediately after the 20 min period of ABS measurements are very similar to that of the "raw" primary particle distribution; it is therefore concluded that the methodology adopted to disaggregate the kaolin in the tank is working satisfactorily. Given how similar the three distributions were, the three were averaged together to form a single distribution that would represent the primary particle distribution in all experiments.

4.1.2. Flocculated Particles

[34] The number of particles identified for each experiment is shown in Table 1. The table shows a large variability in the number of identified particles, which typically increased with concentration. In a number of cases (e.g., 0.2 g/l run1 FL4) the number of identified particles was too low to provided robust estimates of $n(a)$. By visual inspection of all the measured distributions, a minimum threshold of 150 particles was adopted and any distribution that contained fewer than 150 particles was removed from the analysis. The threshold of 150 represents a trade-off between accuracy and including as many distributions as possible. A table containing the coefficients for the log-normal distributions is available online in the supporting information.

4.2. Floc Densities

[35] The estimates of effective density for all identified flocs from across all 15 experiments are shown in Figure 8. All floc effective density estimates were grouped together so that a single relationship between a and $\Delta\rho$ could be derived. Due to the self-similar (fractal) geometry of flocs, a power law relationship between a and $\Delta\rho$ is frequently applied [*Curran et al.*, 2007; *Fennessy et al.*, 1994;

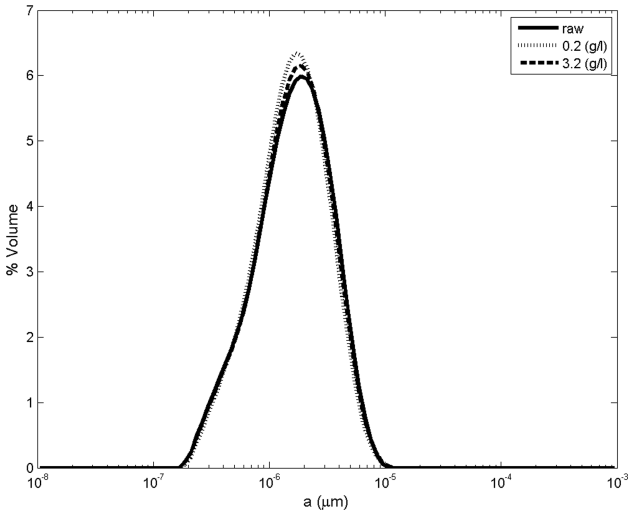

Figure 7. Size distributions of the primary kaolin particles measurement by the Malvern MasterSizer.

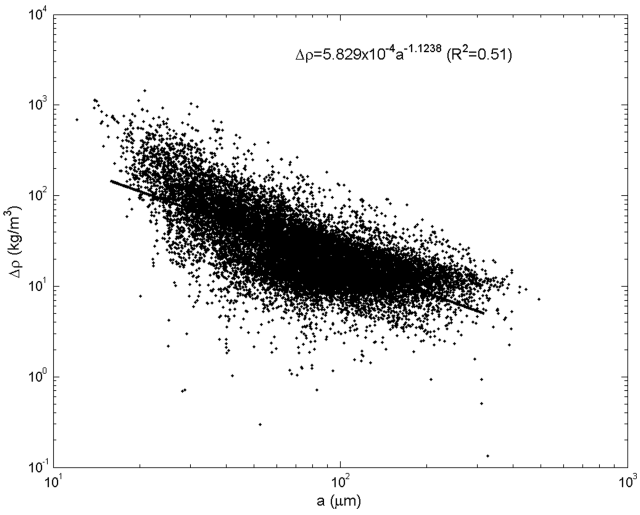

Figure 8. Effective density estimates for all identified flocs from all 15 experiments.

Graham and Nimmo Smith, 2010; *Khelifa and Hill*, 2006]. The solid black line in Figure 8 shows the result of fitting a power law to the measured effective densities.

4.3. η and κ

[36] From a possible 225, 193 valid estimates for η and κ ($R^2 > 0.95$) were obtained from the experiments. Of the 32 experiments that failed to yield valid estimates, 30 of them arose from the suspensions of primary particles. The only valid estimates for η and κ for the runs involving primary particles occurred at mass concentrations of 1.6 and 3.2 g/l. Interestingly, even at low-mass concentrations the transition from primary particles to FL1 was sufficient to produce valid estimates of η and κ, which is potentially significant as it indicates a significant difference in the scattering characteristics of a suspension of primary particles compared to a suspension of flocs. A table containing the experimentally derived values for η and κ, including an estimate of their errors at the 95% confidence interval, is available online in the supporting information.

4.4. Scattering Properties

[37] An important question that can now be addressed is whether the scattering characteristics are controlled by the properties of the flocculated particles or by the constituent primary particles. This is addressed in Figure 9. In this figure, all the valid estimates of K_s are plotted against the mean particle radius, which is defined as

$$a_0 = \int_0^\infty an(a)\mathrm{d}a.$$

[38] In Figure 9 two sets of K_s estimates (derived using equation (7)) are displayed. Here the blue symbols are K_s derived using η obtained from the primary particles experiments and using the properties of the primary particles (e.g., $n(a)$, N and $\rho(a)$). The red symbols are derived using η obtained from the flocculated experiments (FL1–FL4) and the properties of the primary particles. As all K_s estimates shown in Figure 7 use the particle size distribution of the primary particles they all have the same a_0. The idea here is that if the K_s values before aggregation (blue symbols) agree with those obtained after aggregation (red symbols) then the scattering characteristics are controlled by the primary particles and not by the properties of the flocs, but if they are different then the scattering characteristics are influenced by the presence of the flocs.

[39] In order to see if the K_s values are significantly different, error estimates in K_s are also shown in Figure 9. The goal of the error analysis is not to calculate the absolute error in K_s but to provide an assessment of the relative errors between K_s estimates. Equation (9) shows that K_s is a function of η, K_t, and N. As K_t is a constant throughout the experiments it does not contribute to the relative error between K_s estimates. Error estimates in η were derived at the 95% confidence interval. As the primary particle properties $n(a)$ and $\rho(a)$ have been assumed to be constant the relative source of error in estimating N comes from the concentration (M) measurements. To this point it was assumed that the actual concentration lay within 10% of the measured value.

[40] From Figure 9 it is apparent that the two sets of K_s values do not agree, furthermore the differences between the blue and red symbols are significant as the difference between the two is far greater than the variability predicted by the error analysis. This is an important result as it conclusively demonstrates that the acoustic properties of the flocculated particles are not solely controlled by the primary particles; some aspect of the floc structure is influencing the scattering characteristics.

[41] Particularly for the experiments performed at the lower concentrations, it was not possible to generate a complete set of K_s values from primary particle through to FL4. For the experiments in which a complete set of estimates was made the values are listed in Table 2; the numbers in the brackets are the ratio of flocculated K_s to the primary particle K_s. For all the experiments shown in Table 2, K_s shows a monotonic increase with the degree of flocculation.

Table 1. Number of Particles Detected by the Automatic Particle Recognition System[a]

	Run 1				Run 2				Run 3			
	FL1	FL2	FL3	FL4	FL1	FL2	FL3	FL4	FL1	FL2	FL3	FL4
0.2 g/l	**44**	159	**122**	**11**	**31**	164	183	**44**	**46**	**140**	263	**19**
0.4 g/l	**57**	572	**112**	541	**19**	492	203	271	**127**	586	987	261
0.8 g/l	446	636	408	1115	764	450	353	623	261	686	1097	717
1.6 g/l	1082	1105	1350	1004	1915	973	993	1823	1524	1762	2023	1225
3.2 g/l	3707	1349	579	1039	2020	1610	945	630	1814	1027	1398	550

[a]Numbers in bold highlight distributions in which fewer than 150 particles were detected, and that were subsequently excluded from the analysis.

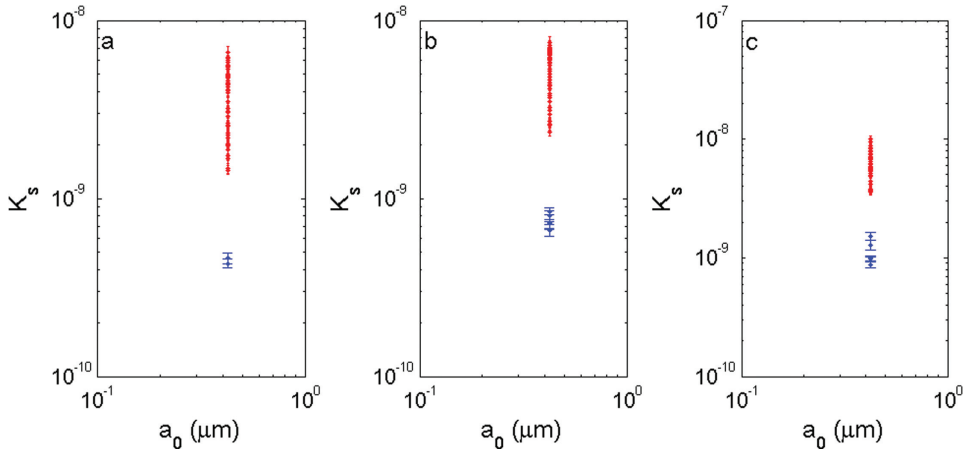

Figure 9. Measurements of K_s, including error bars (see text for explanation on how errors were calculated). The blue symbols are K_s derived using η obtained from the primary particles experiments and using the properties of the primary particles. The red symbols are derived using η obtained from the flocculated experiments (FL1–FL4) and the properties of the primary particles. Panels: (a) 3MHz, (b) 4 MHz, and (c) 5 MHz. The data displayed in this figure are available online in the supporting information.

[42] The results shown in Figure 9 and Table 2 clearly demonstrate that the scattering characteristics of flocculated particles are not solely controlled by the scattering characteristics of the constituent primary particles. Hence, we now investigate K_s and $\overline{\sigma_t}$ in terms of the properties of the flocculated particles. Figure 10 displays $\overline{\sigma_t}$ and K_s for the primary and flocculated distributions. The values for $\overline{\sigma_t}$ and K_s shown in Figure 10 were derived using the corresponding particle properties, e.g., for the flocculated distributions the flocculated particle characteristics are used.

[43] A limitation of our methodology is that inaccurate estimates for $\overline{\sigma_t}$ can be generated for distributions of particles that only weakly backscatter sound (e.g., small particles). This occurs if the measured slope (κ) is comparable to twice the sum of the two attenuation terms (α_v and α_w) (see equation (6)). As a consequence of their small size and the high attenuation due to viscous absorption, no estimates for $\overline{\sigma_t}$ can be derived for the distributions of primary particles.

[44] While Figure 10 shows some variability in the estimates for K_s and $\overline{\sigma_t}$, the trends in the data are clear: K_s and $\overline{\sigma_t}$ both increase as the degree of flocculation increases (as indicated by an increase in a_0). This is most evident when comparing the derived values for K_s for a suspension of flocculated particles to K_s for a suspension of primary particles.

[45] To compare our results with existing noncohesive data sets [*Moate and Thorne*, 2009; *Sheng and Hay*, 1988; *Thorne and Meral*, 2008] K_s and $\overline{\sigma_t}$ were translated to $\langle f \rangle$ and $\langle \chi \rangle$ as follows

$$\langle f \rangle = K_s \sqrt{\frac{a_0}{\int_0^\infty a^3 n(a) da}} \tag{17}$$

$$\langle \chi \rangle = \overline{\sigma_t} \frac{a_0}{2\pi \int_0^\infty a^3 n(a) da} \tag{18}$$

Table 2. K_s Values for the Experiments in Which a Full Set of K_s Values Were Obtained From Primary Particle Through to floc Level 4 (FL4)

Concentration (g/l)	Run	Frequency (MHz)	PP	FL1	FL2	FL3	FL4
1.6	1	4	8.5E-10	3.1E-09 (3.7)	5.8E-09 (6.9)	6.6E-09 (7.8)	7.0E-09 (8.3)
1.6	1	5	9.9E-10	3.6E-09 (3.6)	6.7E-09 (6.8)	7.8E-09 (7.9)	8.4E-09 (8.5)
1.6	2	5	9.7E-10	3.7E-07 (3.8)	6.4E-09 (6.6)	7.5E-09 (7.7)	7.8E-09 (8.1)
1.6	3	4	7.2E-10	2.4E-09 (5.1)	4.8E-09 (10.5)	6.0E-09 (13.1)	6.4E-09 (14.0)
1.6	3	5	8.8E-10	3.8E-09 (8.2)	6.9E-09 (15.1)	7.9E-09 (17.1)	8.0E-09 (17.4)
3.2	1	3	4.6E-10	2.5E-09 (5.5)	5.0E-09 (10.8)	6.2E-09 (13.5)	6.7E-09 (14.4)
3.2	1	4	8.0E-10	3.2E-09 (4.1)	6.4E-09 (8.1)	6.7E-09 (8.5)	7.5E-09 (9.5)
3.2	1	5	1.5E-09	5.7E-09 (3.8)	7.8E-09 (5.2)	9.4E-09 (6.3)	1.0E-08 (6.6)
3.2	2	4	7.4E-10	3.0E-09 (4.1)	5.2E-09 (7.1)	6.8E-09 (9.2)	7.0E-09 (9.5)
3.2	2	5	1.3E-09	5.6E-09 (4.4)	7.9E-09 (6.2)	8.2E-09 (6.5)	8.5E-09 (6.7)
3.2	3	3	4.3E-10	2.6E-09 (6.1)	5.0E-09 (11.5)	6.1E-09 (14.1)	6.2E-09 (14.4)
3.2	3	4	6.6E-10	3.3E-09 (4.9)	5.4E-09 (8.1)	6.9E-09 (10.4)	7.2E-09 (10.9)

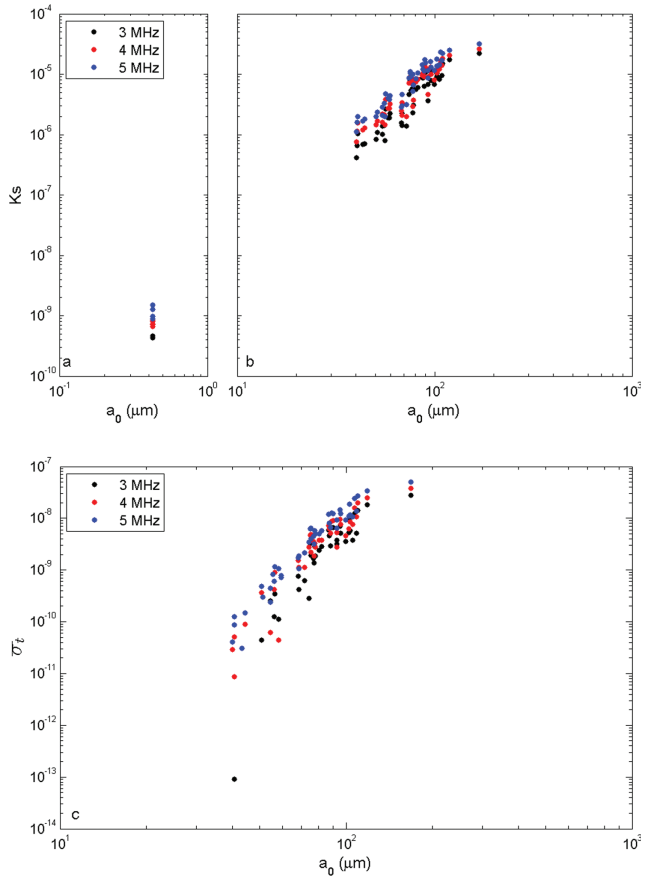

Figure 10. Scattering properties derived from measurements: (a) K_s for primary particles. (b) K_s for flocculated distributions. (c) $\overline{\sigma_t}$ for flocculated particles. The data displayed in this figure are available online in the supporting information.

[46] For the asymptote of a single spherical grain size, equations (17) and (18) reduce to $\langle f \rangle = K_s/a$ and $\langle \chi \rangle = \overline{\sigma_t}/2\pi a^2$ respectively.

[47] The measured scattering properties now reported as $\langle f \rangle$ and $\langle \chi \rangle$ are compared to predictions from the ES and FS models in Figure 11. For the ES model it is assumed that the flocculated particle has the same physical characteristics as a solid kaolin particle. Hence, the values used in the ES model for a kaolin particle were compressional (c_c) and shear wave (c_s) velocities of 2056.9 m/s and 1519.1 m/s, respectively [*Vanorio et al.*, 2003], and a solid density (ρ_s) of 2650 kg/m^3.

[48] For the FS model, the two main parameters that need to be specified are the particle density and the compressional wave speed. Under the assumption of the FS model, a fluid particle cannot support shear waves (i.e., c_s =0). Particle density was supplied via the relationships derived from the FLOCView measurements (see Figure 8). The compressional wave speed in the particle was modeled as

$$c_c = \varphi c_{c,f} + (1 - \varphi) c_s$$

where $c_{c,f}$ is the speed of sound in water (~1500 m/s) and ϕ is the particle porosity, which is defined as

$$\varphi = \frac{\rho_s - \rho_f}{\rho_s - \rho_w}.$$

[49] Because primary particles are solid, no predictions from the FS model were made for that case.

[50] From Figure 11a it is evident that for the suspensions of primary particles the measured values of $\langle f \rangle$ compare favorably to those predicted by the ES model. For a suspension of flocculated particles, Figures 11b and 11c show that the measured values of $\langle f \rangle$ and $\langle \chi \rangle$ tend to collapse onto a single line. Figures 11b and 11c also show that neither the ES nor the FS model adequately represents the scattering characteristics for a suspension of flocculated particles. Generally, the ES model overestimates the measured values of $\langle f \rangle$ and$\langle \chi \rangle$, while the FS model underestimates the measured values of $\langle f \rangle$ and$\langle \chi \rangle$.

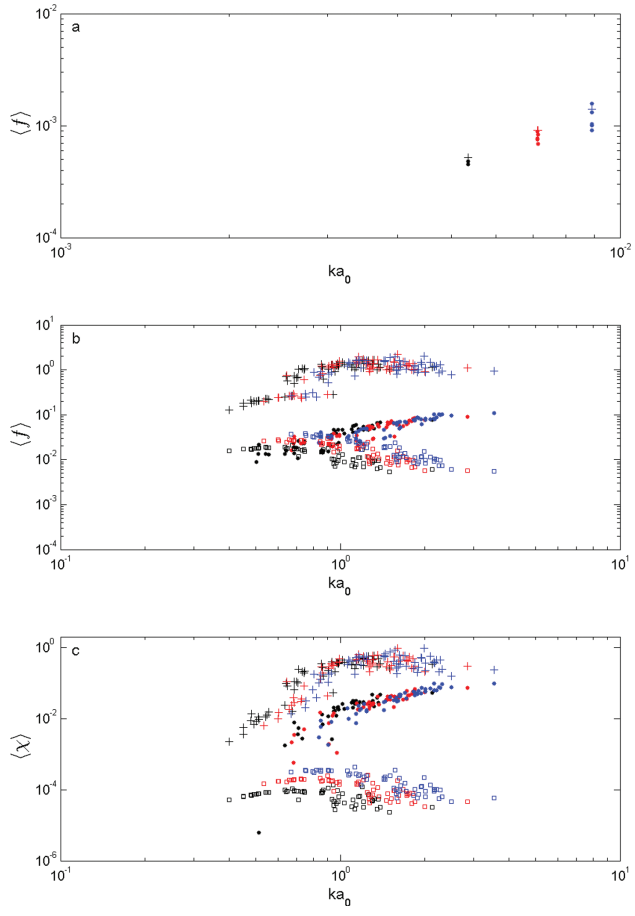

Figure 11. Model-data comparisons. (a) $\langle f \rangle$ for primary particles. (b) $\langle f \rangle$ for flocculated distributions. (c) $\langle \chi \rangle$ for flocculated particles. Colors represent transducer frequency: 3MHz (black), 4MHz (red) and 5 MHz (blue). The symbols represent: • Data, + ES model and □ FS model. The data displayed in this figure are available online in the supporting information.

5. Discussion

5.1. Ensemble Backscatter Form Function (K_s)

[51] The results presented here have shown that the scattering properties of cohesive fine sediments are greatly affected by the flocculation process. The results have conclusively demonstrated that the constituent primary particles do not control the scattering characteristics of a suspension the flocculated particles. The overall trend is for K_s to increase as the degree of flocculation increases, at least over the range of a_0 values presented here.

5.2. Total Scattering Cross Section ($\overline{\sigma_t}$)

[52] In calculating $\overline{\sigma_t}$ for a suspension of flocculated particles it was assumed that the attenuation due to viscous absorption was negligible. Treating the flocs as solid particles with reduced density might not be a good approximation and, as a consequence, viscous absorption may still be important. If this were the case then the values for $\overline{\sigma_t}$ shown in Figure 10c would be an overestimate, as some of the attenuation which was attributed to particle scattering would in fact have resulted from viscous absorption.

[53] The magnitude of viscous losses depends on the relative motion of the fluid and the particle [*Hay and Burling*, 1982]. In the case of flocs, the decrease in floc density with size, results in a decrease in the floc's particle relaxation time, which can be thought of as a measure of the particle's inertia with respect to the motion of the fluid. Given a reduction in the floc's density with size it would seem unlikely that viscous absorption would increase with floc size. That leaves two possibilities: the first is that the viscous absorption is controlled by the properties of primary particles and is therefore invariant with increasing floc size, and second that the losses from viscous absorption decrease with increasing floc size. If the viscous absorption is constant with size then, while an overestimate, the observed trend in $\overline{\sigma_t}$ would remain unchanged. If the viscous absorption decreases with increasing floc size then the trends shown in Figure10c do not relate to $\overline{\sigma_t}$ but to a combination of $\overline{\sigma_t}$ and α_v. Understanding how α_v (and therefore $\overline{\sigma_t}$) changes with the degree of flocculation warrants further research.

[54] In natural energetic environments dominated by flocculated sediment, flocs have been observed to adjust their size to stay in equilibrium with the local smallest turbulent eddy length scale, i.e., the Kolmogorov microscale [*Fugate and Friedrichs*, 2003] so there remains a possibility that the floc size distribution evolved while the sample was transferred from the highly turbulent recirculation tank, via the pipette, to the quiescent FLOCview chamber. The greatest growth between the recirculation tank and the FLOCview chamber might be expected for the largest flocs, because they would be the most likely to have been broken up by shear in the recirculation tank and then could reform as shear disappeared in the pipette and FLOCView chamber. As the FLOCView chamber is initially filled with particle free water, flocs settling into the FLOCview chamber experience a significant reduction in the floc concentration. In turn, this reduction greatly reduces the chances of floc collisions resulting from differential settling. Given the quiescent nature of the FLOCview chamber differential settling would be the dominate flocculation mechanism. To this point, visual observations of flocs settling in the FLOCView chamber indicate that aggregation resulting from differential settling is negligible. While it is possible that floc evolution occurs within the pipette, the short residence time of the flocs while in the pipette would greatly limit the possibility of additional flocculation. Unfortunately, we have no way of checking on this evolution but, if it did occurred then the size distribution of flocs in the recirculation tank would be smaller than that measured by FLOCView, and hence values shown in Figure 10 for K_s and $\overline{\sigma_t}$ would be an overestimate.

5.3. Model-Data Comparison

[55] The observations show that neither the ES nor the FS models in their current form are capable of adequately predicting the scattering characteristics of a suspension of flocculated particles. These two models were selected as they potentially span the transition from solid (primary) particles to large fluid-like flocs. While the two models did provide upper (ES) and lower (FS) bounds to the measurements, the transition from solid to fluid-like particles did not follow expectations. It would seem reasonable to hypothesize that the ES model would work better on the suspension of primary particles, and then as flocculation took place, the measurements would tend toward the FS predictions. If anything, the observations tend more toward the predictions of the ES model as the degree of flocculation increases.

[56] Although the observations show that neither the ES nor the FS model is a good predictor for the backscatter from flocs, there are some very encouraging signs which suggest the ABS may be a useful tool for measuring the concentration of flocculated sediment. Observed $\langle f \rangle$ values for primary particles are close to those predicted by the ES model. In terms of the flocculated particles, the most promising feature is how the observations for $\langle f \rangle$ and $\langle \chi \rangle$ collapse onto a single curve (when plotted against x). From this it would seem reasonable to assume that flocs scatter sound in a systematic and predictable fashion. Given the rather disappointing performance of both the ES and FS models in their existing form, a new theoretical scattering model for flocculated particles is required. Progress is required in two fundamental areas. First, the scattering model must incorporate an intrinsic feature of flocculated particles, this being the observed decrease in floc density with increasing floc size. Second, investigations are required to identify what type of waves propagate in flocs: compressional or shear or both? Furthermore, an important aspect of this work will be developing relationships that predict how C_c and C_s vary with floc density.

[57] The starting point for incorporating the decrease in floc density with increasing floc size in the scattering model is to describe flocs as fractal objects [*Dyer and Manning*, 1999; *Jiang and Logan*, 1991; *Kranenburg*, 1994; *Lee et al*., 2002; *Li et al*., 1998, 2004]. The key relationship when using a fractal description of flocs is that the mass of a floc (m_f) scales with the floc diameter (d) as

$$m_f \propto d^{D_f},$$

where D_f is the fractal dimension.

[58] Using a fractal description *Lee et al*. [2000] developed expressions for various floc properties. The

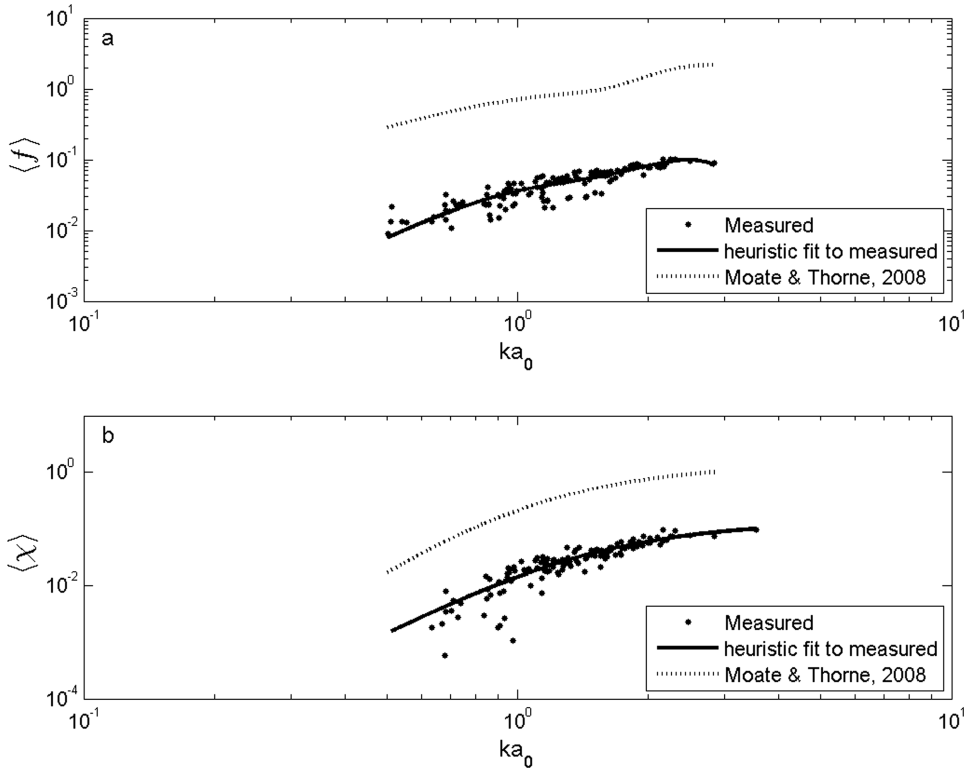

Figure 12. Results of fitting measured values of (a) $\langle f \rangle$ and (b) $\langle \chi \rangle$ to the heuristic expression of *Moate and Thorne* [2008].

expression of most interest here is the density-size relationship which is given by

$$\rho_f = \rho_s \left(\frac{d}{d_0} \right)^{D_f - 3},$$

where d_0 is the diameter of the primary particles. Incorporating this type of equation into scattering equations would produce the required density-size dependence.

[59] In the theory outlined by *Buckingham* [2000] for wave propagation in saturated, unconsolidated marine bed sediments, algebraic expressions for C_c and C_s, which are functions of sediment porosity and acoustic frequency, are derived. The application or the adaptation of these expressions to flocculated particles warrants further consideration.

5.4. Operational Considerations

[60] In terms of the purely operational use of acoustics for measuring the concentration of flocculated sediments, an empirical or heuristic relationship could be fitted to the observations. Such an approach is routinely used for determining the scattering characteristics of noncohesive sediments [*Moate and Thorne*, 2009; *Sheng and Hay*, 1988; *Thorne and Hanes*, 2002].

[61] Figure 12 shows the results of fitting our measured values of $\langle f \rangle$ and $\langle \chi \rangle$ for flocculated distributions to the heuristic expressions proposed by *Moate and Thorne* [2009] (their equations (22) and (23)). From Figure 12 it is apparent that a reasonable fit between measurements and the expression of *Moate and Thorne* [2009] can be achieved. This result highlights the potential suitability of such an approach for a suspension of flocculated particles. The dashed line in Figure 12 shows the expression of *Moate and Thorne* [2009] derived from measurements of a suspension of quartz sediments. A comparison of the dashed and solid line shows that the values for $\langle f \rangle$ and $\langle \chi \rangle$ for flocculated kaolin particles are several orders of magnitude smaller than those for quartz sediments. This result clearly demonstrates that expressions derived for quartz are not suitable for use on flocculated particles. From a sedimentologist's point of view, it is use of $\langle f \rangle$ and $\langle \chi \rangle$ in the inverse problem [*Lee and Hanes*, 1995; *Moate and Thorne*, 2009; *Thorne and Hanes*, 2002; *Thosteson and Hanes*, 1998] which yields estimates of concentration and particle size that is of primary interest.

[62] In terms of estimating concentration and particle size from a suspension of flocculated kaolin particles the heuristic expressions derived for $\langle f \rangle$ and $\langle \chi \rangle$ in this study could form the basis of such an inversion. However, until a better theoretical understanding of how sound interacts with flocculated particles is achieved, the fitting of such empirical relations may be somewhat premature.

6. Conclusions

[63] The measurements presented here have shown that the scattering properties of cohesive fine sediments are greatly affected by the flocculation process. Perhaps the most fundamental result is that the measurements have conclusively demonstrated that the constituent primary particles do not solely control the scattering characteristics of a suspension the flocculated particles.

[64] Over the range of floc sizes investigated here, the overall trend is for the ensemble backscatter form function (K_s) to increase as the degree of flocculation increases. This trend was also observed in total scattering cross section ($\overline{\sigma_t}$) but this result is dependent on the assumption that viscous absorption for flocculated particles is negligible. Further investigation on how viscous absorption is affected by flocculation is a key research question that merits further consideration.

[65] The results have also shown that, in their current form, neither the elastic or the FS model is capable of adequately representing the scattering characteristics of a suspension of flocculated particles, although the two models did provide upper (ES) and lower (FS) bounds to the measurements.

[66] In terms of the operational use of acoustics to measure the concentration of flocculated sediments, empirical or heuristic relationships could be fitted to the observations but, until a better theoretical understanding of how sound interacts with flocculated particles is achieved, the fitting of such empirical relations may be somewhat premature.

Appendix A: Model Terms

[67] For the ES model b_q is given [*Gaunaurd and Überall*, 1983]

$$b_q = \frac{\begin{vmatrix} \beta_1 & \alpha_{12} & \alpha_{13} \\ \beta_2 & \alpha_{22} & \alpha_{23} \\ 0 & \alpha_{32} & \alpha_{33} \end{vmatrix}}{\begin{vmatrix} \alpha_{11} & \alpha_{12} & \alpha_{13} \\ \alpha_{21} & \alpha_{22} & \alpha_{23} \\ 0 & \alpha_{32} & \alpha_{33} \end{vmatrix}},$$

and

$$\beta_1 = -x_t^2(\rho_w/\rho_s)j_q(x), \beta_2 = xj'_q(x),$$

$$\alpha_{11} = x_t^2(\rho_w/\rho_s)h_q^{(1)}(x), \alpha_{12} = -xh'^{(1)}_q(x),$$

$$\alpha_{12} = \left[2q(q+1) - x_t^2\right]j_q(x_l) - 4x_l j'_q(x_l),$$

$$\alpha_{22} = xj'_q(x_l), \alpha_{32} = 2\left[j'_q(x_l) - x_l j'_q(x_l)\right],$$

$$\alpha_{13} = 2q(q+1)\left[xj'_q(x_t) - j_q(x_t)\right], \alpha_{23} = q(q+1)j_q(x_t),$$

$$\alpha_{33} = 2xj'_q(x_t) + j_q(x_t)\left[x_t^2 - 2q(q+1) + 2\right],$$

$$x = ka, x_t = x(c/c_s), x_l = x(c/c_c),$$

where j_q is the spherical Bessel function, $h_q^{(1)}$ is the Hankel function, the primes denote first derivatives, c is the speed of sound in the fluid, c_s and c_c are the shear and compressional wave speeds respectively, ρ_w is the fluid density and ρ_s is the density of the particle.

[68] For the FS model c_q is given by *Anderson* [1950]

$$c_q = \frac{\left(\alpha_q(x_p)/\alpha_q(x)\right)\left(n_q(x)/j_q(x_p)\right) - \left(\beta_q(x)/\alpha_q(x)\right)\left(\rho_p/\rho_w\right)(c_p/c)}{\left(\alpha_q(x_p)/\alpha_q(x)\right)\left(j_q(x)/j_q(x_p)\right) - \left(\rho_p/\rho_w\right)(c_p/c)},$$

and

$$\alpha_q(x) = qj_{q-1}(x) - (q+1)j_{q+1}(x)$$
$$\beta_q(x) = qn_{q-1}(x) - (q+1)n_{q+1}(x),$$

$$x_p = k_p a,$$

where n_q is the spherical Neumann function, k and k_p are the wave number in the fluid medium and in the FS respectively, ρ_p is the density of the FS, c_p is the speed of sound in the FS, and all other terms are previously defined.

[69] **Acknowledgments.** This work is supported by the UK Natural Environment Research Council project FLOCSAM. The authors would like to acknowledge their coresearchers at the University of Plymouth. I.T.M. would like to thank G. Flowerdue and S. Rix for manufacturing several parts for the recirculation tank. We would also like to thank Malcom Green for his valuable input into the manuscript. The authors would like to thank the reviewers of an earlier version of this paper for their valuable comments and suggestions which have been incorporated into this revised version.

References

Anderson, V. C. (1950), Sound scattering from a fluid sphere, *J. Acoust. Soc. Am.*, *22*(4), 426–431.

Betteridge, K. F. E., P. D. Thorne, and R. D. Cooke (2008), Calibrating multi-frequency acoustic bacKscatter systems for studying near-bed suspended sediment transport processes, *Cont. Shelf Res.*, *28*, 227–235.

Buckingham, M. J. (2000), Wave propagation, stress relaxation, and grain-to-grain shearing in saturated, unconsolidated marine sediments, *J. Acoust. Soc. Am.*, *108*(6), 2796–2815.

Curran, K. J., P. S. Hill, T. G. Milligan, O. A. Mikkelsen, B. A. Law, X. Durrieude Madron, and F. Bourrin (2007), Settling velocity, effective density, and mass composition of suspended sediment in a coastal bottom boundary layer, Gulf of Lions, France, *Cont. Shelf Res.*, *2007*, 1408–1421.

Deines, K. L. (1999), Backscatter estimation using broadband acoustic Doppler current profilers, *Proc. Sixth Working Conf. on Current Measurement*, San Diego, CA, IEEE, 249–253.

Downing, A., P. D. Thorne, and C. E. Vincent (1995), Backscattering from a suspension in the near field of a piston transducer, *J. Acoust. Soc. Am.*, *97*(3), 1614–1620.

Dyer, K. R., and A. J. Manning (1999), Observation of the size, settling velocity and effective density of flocs, and their fractal dimensions, *J. Sea Res.*, *41*, 87–95.

Eisma, D., P. Bernard, G. C. Cadee, V. Ittekkot, J. Kalf, R. Laane, J. M. Martin, W. G. Mook, A. van Put, and T. Schuhmacher (1991), Suspended-matter particle size in some West-European estuaries; PART II: A review on the floc formation and break-up, *Neth. J. Sea Res.*, *28*(3), 215–220.

Fennessy, M. J., K. R. Dyer, and D. A. Huntley (1994), INSSEV: An instrument to measure the size and settling velocity of flocs in situ, *Mar. Geol.*, *117*, 107–117.

Fugate, D. C., and C. T. Friedrichs (2002), Determining concentrations and fall velocity of estuarine particle populations using ADV, OBS and LISST, *Cont. Shelf Res.*, *22*, 1867–1886.

Fugate, D. C., and C. T. Friedrichs (2003), Controls on suspended aggregate size in partially mixed estuaries, *Estuarine Coastal Shelf Sci.*, *58*, 389–404.

Gaunaurd, G. C., and H. Überall (1983), RST analysis of monostatic and bistatic acoustic echoes from an elastic sphere, *J. Acoust. Soc. Am.*, *73*(1), 1–12.

Graham, G. W., and W. A. M. Nimmo Smith (2010), The application of holography to the analysis of size and settling vleocity of suspended cohesive sediments, *Limnol. Oceanogr.*, *8*, 1–15.

Hay, A. E., and R. W. Burling (1982), On sound scattering and attenuation in suspensions, with marine applications, *J. Acoust. Soc. Am.*, *72*(3), 950–959.

Jiang, Q., and B. E. Logan (1991), Fractal dimensions of aggregates determined from steady-state size distributions, *Environ. Sci. Technol.*, *25*(12), 2031–2038.

Khelifa, A., and P. S. Hill (2006), Models for effective density and settling velocity of flocs, *J. Hydraul. Res.*, *44*(3), 390–401.

Kranenburg, C. (1994), The fractal structure of cohesive sediment aggregates, *Estuarine Coastal Shelf Sci.*, *39*, 451–460.

Lee, D. G., J. S. Bonner, L. S. Garton, A. N. S. Ernest, and R. L. Autenrieth (2000), Modeling coagulation kinetics incorporating fractal theories: a fractal rectilinear approach, *Water Res.*, *34*(7), 1987–2000.

Lee, D. G., J. S. Bonner, L. S. Garton, A. N. S. Ernest, and R. L. Autenrieth (2002), Modeling coagulation kinetics incorporating fractal theories: comparison with observed data, *Water Res.*, *36*(4), 1056–1066.

Lee, T. H., and D. M. Hanes (1995), Direct inversion method to measure the concentration profile of suspended particles using backscattered sound, *J. Geophys. Res.*, *100*(C2), 2649–2657, doi:10.1029/94JC03068.

Li, X., U. Passow, and B. E. Logan (1998), Fractal dimensions of small (15–200 μm) particles in Eastern Pacific coastal waters, *Deep Sea Res. Part I*, *45*(1), 115–131.

Li, X., J. Zhang, and J. H. W. Lee (2004), Modelling particle size distribution dynamics in marine waters, *Water Res.*, *38*(5), 1305–1317.

Manning, A. J., and K. R. Dyer (1999), A laboratory examination of floc characteristics with regard to turbulent shearing, *Mar. Geol.*, *160*(1-2), 147–170.

Manning, A. J., and K. R. Dyer (2002), The use of optics for the in situ determination of flocculated mud characteristics, *J. Opt. A Pure Appl. Opt.*, *4*(4), S71–S81.

Manning, A. J., and S. J. Bass (2006), Variability in cohesive sediment settling fluxes: Observations under different estuarine tidal conditions, *Mar. Geol.*, *235*(1–4), 177–192.

Mikkelsen, O. A., P. S. Hill, T. G. Milligan, and R. J. Chant (2005), In situ particle size distributions and volume concentrations from a LISST-100 laser particle sizer and a digital floc camera, *Cont. Shelf Res.*, *25*(16), 1959–1978.

Moate, B. D., and P. D. Thorne (2009), Measurements and inversion of acoustic scattering from suspensions having broad size distributions, *J. Acoust. Soc. Am.*, *126*(6), 2905–2917.

Otsu, N. (1979), A threshold selection method from gray-level histograms, *IEEE Trans. Syst. Man Cybern.*, *9*(1), 62–66.

Richards, S. D., A. D. Heathershaw, and P. D. Thorne (1996), The effect of suspended particulate matter on sound attenuation in seawater, *J. Acoust. Soc. Am.*, *100*(3), 1447–1450.

Sheng, J., and A. E. Hay (1988), An examination of the spherical scatterer approximation in aqueous suspensions of sand, *J. Acoust. Soc. Am.*, *83*(2), 598–610.

Smith, S. J., and C. T. Friedrichs (2011), Size and settling velocities of cohesive flocs and suspended sediment aggregates in a trailing suction hopper dredge plume, *Cont. Shelf Res.*, *31*(10, Suppl.), S50–S63.

Thorne, P. D., and D. M. Hanes (2002), A review of acoustic measurement of small-scale sediment processes, *Cont. Shelf Res.*, *22*(4), 603–632.

Thorne, P. D., and M. J. Buckingham (2004), Measurement of scattering by a suspension of irregularly shaped sand particles and comparison with a single parameter modified sphere model, *J. Acoust. Soc. Am.*, *116*(5), 2876–2889.

Thorne, P. D., and R. Meral (2008), Formulations for the scattering properties of suspended sandy sediments for use in the application of acoustics to sediment transport processes, *Cont. Shelf Res.*, *28*(2), 309–317.

Thosteson, E. D., and D. M. Hanes (1998), A simplified method for determining sediment size and concentration from multiple frequency acoustic bacKscatter measurements, *J. Acoust. Soc. Am.*, *104*(2), 820–830.

Urick, R. J. (1948), The absorption of sound in suspensions of irregular particles, *J. Acoust. Soc. Am.*, *20*(3), 283–289.

Vanorio, T., M. Prasad, and A. Nur (2003), Elastic properties of dry clay mineral aggregates, suspensions and sandstones, *Geophys. J. Int.*, *155*(1), 319–326.

Winterwerp, J. C. (2002), On the flocculation and settling velocity of estuarine mud, *Cont. Shelf Res.*, *22*(9), 1339–1360.